Lab on a Chip

Accepted Manuscript

ROYAL SOCIETY OF CHEMISTRY

www.rsc.org/loc

Journal Name

ARTICLE

The intercell dynamics of T cells and dendritic cells in a lymph node-on-a-chip flow device

Received 00th January 20xx,
Accepted 00th January 20xx

DOI: 10.1039/x0xx00000x

www.rsc.org/

Patrícia Moura Rosa,[a,c] Nimi Gopalakrishnan,[a,c] Hany Ibrahim,[b] Markus Haug[b] and Øyvind Halaas*[a]

T cells play a central role in immunity towards cancer and infectious diseases. T cell responses are initiated in the T cell zone of the lymph node (LN), where resident antigen-bearing dendritic cells (DCs) prime and activate antigen-specific T cells passing by. In the present study, we investigated the T cell:DC interaction in a microfluidic device to understand the intercellular dynamics and physiological conditions in LN. We show random migration of antigen specific T cells on antigen presenting DC monolayer independent of flow direction with mean T cell:DC dwell time of 12.8 min and mean-velocity of 6 µm/min. Furthermore, we investigated the antigen specific *vs.* unspecific attachment and detachment of $CD8^+$ and $CD4^+$ T cell to DCs under varying shears stress. In our system, $CD4^+$ T cells showed long stable contacts with APCs whereas $CD8^+$ T cells presented transient interactions with DCs. By varying the shear stress from 0.01 to 100 Dyn.cm^{-2}, it was also evident that there was a much stronger attachment of antigen-specific than unspecific T cells to stationary DCs up to 1-12 Dyn.cm^{-2}. The mechanical force of the cell:cell interaction associated with pMHC-TCR match under controlled tangential shear force was estimated to be in the range of 0.25-4.8 nN. Finally, performing attachment & detachment tests, there was a steady accumulation of antigen specific $CD8^+$ T cells and $CD4^+$ T cells on DCs at low shear stresses, which were released at stress of 12 Dyn.cm^{-2}. This microphysiological model provides new possibilities to recreate controlled mechanical forces threshold of pMHC-TCR binding, allowing to investigate intercellular signalling of immune synapses and therapeutic targets for immunotherapy.

Introduction

Immunoengineering is an emerging field that links biology, pharmaceutics, biomedicine and biophysics with engineering aiming at developing new strategies for molecular and cellular immunotherapies (1). The immune system is particularly suited for engineering approaches due to the natural and dynamic self-governing of the cells involved in initiating an immune response. The immune system is a complex process involving many cell types, responses and microenvironments in several anatomical sites and immunological organs. In response to inflammatory signals, tissue-resident dendritic cells (DCs) acquire local antigens and migrate to lymph nodes to present MHC-bound peptide antigens to T cells recruited from blood. The adaptive immune response is then initiated by the cognate physical interactions between naïve T cells and antigen-presenting cells (APCs). Later, the primed/activated T cells enter the lymph and blood and are recruited to inflammation sites where new T cell:target cell interactions take place. Although numerous *in vivo* and *in vitro* studies describe the molecules and responses involved in these interactions, a comprehensive understanding of the lymph node immune physiology and dynamics considering physical parameters (i.e. influence of shear stress, the duration and stability of the interaction, the magnitude of force sustained at the T cell-APC interface, the relative motions between the two plasma membranes at the T cell-DC interface, number of sequential T cell:DCs interactions, recirculation requirements) underlying molecular mechanisms to achieve priming, activation and proliferation is still not understood (1-4).

Conventional techniques involved in the study of cell interaction dynamics and their behaviour inside lymph nodes such as dissection, confocal microscopy and intravital multiphoton microscopy have been used in the analysis of LN in mice, rat, sheep and humans (3, 5, 6), albeit with severe limitations in access and control (5, 7). On the other hand, traditional cell culture dish systems are lacking proper promoters for migration, intracellular signalling, proliferation, and differentiation because of the absence of extracellular matrix (ECM) (1, 8, 9), the presence of haptotactic gradients (2), shear stress and other hemodynamic forces (1, 10), which are important for successful T cell:DC interaction. To better understand the specialized junction between a T lymphocyte and APC, the immunological synapse formation and the induction of efficient T cell activation, it is also important to consider that the mechanical forces are an integral part of T

[a] Department of Cancer Research and Molecular Medicine, Norwegian University of Science and Technology, 7489 Trondheim, Norway
[b] Centre of Molecular Inflammation Research (SFF-CEMIR), Department of Cancer Research and Molecular Medicine, Norwegian University of Science and Technology, 7489 Trondheim, Norway
[c] NTNU Nanolab, Norwegian University of Science and Technology, 7489 Trondheim, Norway
E-mail: oyvind.halaas@ntnu.no
† Electronic Supplementary Information (ESI) available.
See DOI: 10.1039/x0xx00000x

cell:APC physiology and driving force to the mechanism of TCR triggering by pMHC (11-15), and recent studies in cell-cell adhesion in micropipette aspiration techniques (16) and atomic force microscope (AFM) (17) have been developed. One particular technique that has also been stablished as an important tool for the study of cell adhesion is single-cell force spectroscopy (SCFS) by AFM, allowing the process analysis under near-physiological conditions (18, 19). However, AFM is limited in the investigation of long-term adhesion, considering the characteristic dynamic motile and interaction between T cell:APC during the synapse formation.

To overcome these limitations and to find important cues to better understand the process of T cell:DC interaction during immune responses, we pursued a simple lymph node mimetic microfluidic system. These systems are becoming important to model physiological functions of tissues or organs in 3D over time.

In recent years attention has been focused on additional strategies for understanding the dynamic immune cell interactions. Recently, several studies with monolayers of heterotypic cell-cell interactions have demonstrated that combining the fluid flow with mechanical forces similar to those found *in vivo* can affect cell shape, function, interaction and differentiation process (1, 20-25). These methods and techniques address some questions related to effects of biochemical treatments and environmental *stimuli* to the cell adhesion and cell:cell interaction, offering the potential of monitoring, studying and profiling stem cell interaction, multistep adhesion cascade of entry of lymphocytes through high endothelial venules (HEVs) (rolling, sticking, crawling, transmigration) (24), cancer metastasis. Additionally, these techniques can be also used as therapeutic target for different drugs (1, 23, 26-28).

At single-cell level of cell:cell interactions, five main classes of microscale tools have been described; microwell arrays, valved microfluidics, droplet microfluidics, microfluidic cell trap arrays (29) and electrical cell manipulation (30). Dura *et al.* reported one particular study with microfluidic cell trap array, an approach to demonstrate dynamic interactions between CD8 T cells and APC, to perform measurements on both patterns and to characterize the activation process of CD8 T cells (31).

In this study, we developed a microfluidic platform allowing real-time study of flowing lymphocytes dynamically interacting with adherent dendritic cells. This new technique lays the foundation for studies of cell-cell interaction dynamics during variable velocity, shear stress, deformation rates and migratory motility in different biological settings relevant for the adaptive immune system.

The shear stress of interest in this study relates to the shear stress inside the T cell zones of LNs (3), where in the presence of cognate antigen, T cells arbitrarily migrate along the fibroblastic reticular cell (FRC) network to contact the cognate antigen presented by adherent APCs. During this stage, T cell speed decreases and turning behavior increases, resulting in serial contacts with multiple DCs for 2h (2, 3, 32-39). Interstitial flow velocity measured in normal and tumor-associated inflamed skin range from 0.005 to 0.05 Dyn.cm^{-2} (33), which served as our guide for choosing shear stresses representing physiological conditions, but we also probed the shear stress tolerance in our system.

We first investigated the T cell behavior on DC monolayer under low flow rates. Next we investigated the flow rates needed to break the cell:cell interactions and the DC adherence to the fibronectin surface. Finally we investigated the antigen-specific attachment of T cells to DCs during continuous flow. This study demonstrates that this microfluidic platform can be a valuable tool for investigating T cells:APC interactions related to cell signaling and activation highly relevant for immunological R&D.

1. Materials and Methods

A. Cells

Adherent murine tumor Dendritic Cells (MutuDC; expressing GFP) lines derived from spleen tumors in CD11c:SV40LgT-transgenic C57BL/6 mice were from Hans Acha-Orbea, University of Lausanne; and non-adherent ovalbumin specific MHC class II restricted (MF2.2D9) CD4$^+$ T cell (here after referred to as OVAII) and MHC class I restricted (RF33.70) CD8$^+$ T cell hybridomas (here after referred to as OVAI) were a gift from Dr Kenneth Rock, University of Massachusetts, Worcester. MutuDC lines cells were cultured in 75 cm^2 cell culture flasks with culture medium (CM) composed by IMDM media containing 8% Fetal Calf serum (FCS), 10 mM HEPES, 1.7% L-glutamine, 0,1 µM ciprofloxacin, with 50 µM 2-mercaptoethanol (2-Me), considering the minor modification for this cell type according to (40). MF2.2D9 and RF33.70 T cell with were cultured in 75 cm^2 cell culture flasks with complete growth medium consisting of RPMI-1640 cell medium, mixed with 50 µM 2-Me, 20mM HEPES, glutamine, 10% FCS and antibiotics (CIPRO) (41).

B. Peptide preparation

OVA peptides and variants were purchased from BioSite, Anaspec. All peptides were dissolved in dimethyl sulfoxide (10 mg/ml) and stored at -20°C.

C. Fabrication of a microfluidic system

The microfluidic device was fabricated in polydimethylsiloxane (PDMS) by rapid prototyping soft lithography using SU-8 photoresist masters, according to published procedures (42). The microchannel was designed using AutoCAD 2014 drawing software (Autodesk Inc., Europe). To form the optical mask, a film negative with the desired size of microchannel was prepared by a commercial photomask manufacturer (Compugraphics Ltd, UK), and it was purchased on a soda line photolithography mask (3"x3"x0.060") coated with a thin chrome metal layer. Master for the microfluidic device was fabricated using a two-layer SU-8 process. A 7 µm-thin layer of photoresist (SU-8 5, MicroChem) was used as an adhesion layer and it was spun at 2000 rpm for 120 sec over a 2 inch Si wafer. The wafer was then fully exposed to ultraviolet light (UV light). After a post-exposure baking (1 min at 65°C + 1 min at 95°C), the second layer of photoresist (SU-8 2100, MicroChem) was spun at 4000 rpm for 30 sec to yield feature

heights of 100 µm. The wafer was exposed to UV light through the mask to generate the microchannel patterns. After post-exposure bake (5 min at 65°C and 12 min at 95°C) and development, the mold was hard-baked for 20 min at 150°C.

To produce the PDMS replica, SylgardTM 184 (Dow Corning) silicone was mixed with the curing agent in a proportion of 1:10, poured over the mold and baked at 70°C for 2 h. After curing, the PDMS was peeled from the mold, individual devices were cut to proper sizes and a needle with a blunt tip was used to make the fluid connection access holes. The individual devices were cleaned with acetone and ethanol (70%) and dried with nitrogen. The PDMS replica was irreversibly sealed to a cover glass (from Menzel Gläser, Ø 50 mm dia, 150 µm thickness, compatible with high numerical aperture (high-NA) fluorescence imaging), using plasma cleaner for surface activation. The devices were further mounted onto 1 mm high WillCo-dish®.

The bottom of the channel were coated with collagen (Col) (50 µg/ml, diluted with 1x PBS) or fibronectin (FN) (50 µg/ml, diluted with PBS; Bio-Techne, R&D Systems Europe Limited) to form a matrix for cell attachment (8), and incubated at 4°C overnight. After coating, the device was washed 3 times with PBS, loaded with culture medium, and finally incubated at 37°C and 5% CO_2 for 2 h. Figure 1(a) shows the microfluidic device fabricated as described above and following the insertion of metal catheters (Instech Solomon, ID = 0.8 mm) into the access holes in the PDMS and coupling to polyethylene tubes (Instech Solomon). The microfluidic device includes two inlets and outlets feeding a main microchannel, as illustrated in Figure 1(b). The main microchannel is 10 mm long, 1000 µm wide, and 100 µm height, and one ruler was defined along the side of the channel to facilitate the identification of a particular site of microchannel when using the optical microscope (43).

D. Simulation of wall shear stress and further validation by experimental conditions

COMSOL Multiphysics 4.4 software was used to simulate the wall shear stress (WSS) profile in the microfluidic structure used in this study. This finite elements simulation solved the Navier-Stokes equation (assuming non-slipping walls) to calculate the velocity profile inside a rectangular channel (height=0.01 cm and width=0.1 cm). Then, assuming a constant dynamic viscosity along the channel, the profile of shear stress can be calculated along the rectangular cross section using Eq. (1), where τ is the shear stress in Dyn.cm^{-2}, μ the dynamic viscosity in Dyn.s.cm^{-2} (for cell medium at 37°C, 0.78x10^{-2} Dyn.s.cm^{-2} (9)), u the velocity of the fluid along the boundary cm.s^{-1}, and y the height above the boundary cm.

$$\tau(y) = \mu \frac{\partial u}{\partial y} \qquad (1)$$

Different flow rates, ranging from 100 nL/min to 1000 µL/min, were applied at the inlet and the atmospheric pressure (1.01295x 10^{6} Dyn.cm^{-2}) as imposed at the outlet.

E. Antigen-presentation assays, cell staining and loading procedure, and microfluidic setup

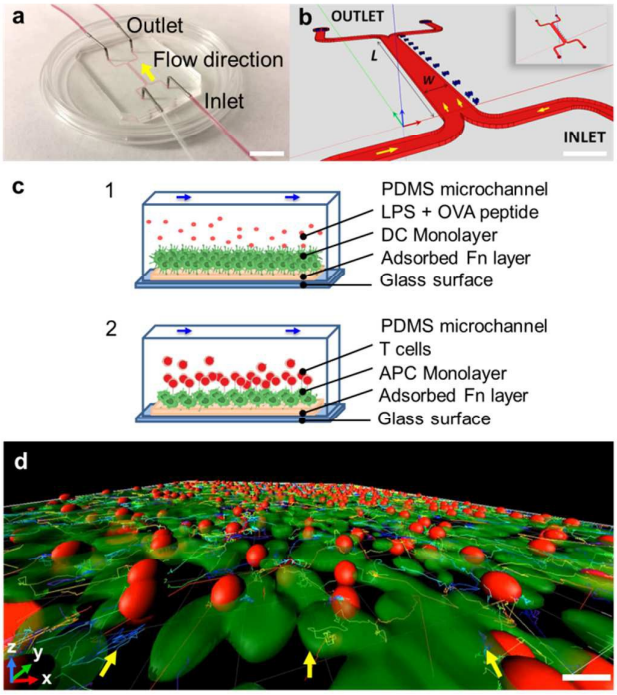

Figure 1| Microfluidic device for immune cell-cell interactions. a) The PDMS biochip on a glass substrate. **b)** The device is composed of one main flow channel and with 2 inlets and 2 outlets. Dimensions of microchannel: length 10 mm, width 1 mm, and height 100 µm. The direction of the flow is indicated by yellow arrows. **c)** Dynamic DC:T-cell interactions during flow. Cross-section view of microchannel: **(1)** Dendritic monolayer and LPS and OVA peptide activation in order to mimic an inflammatory biochemokine response. **(2)** T cell loading and T cell:DCs interaction. Arrow indicates flow direction. **d)** Representation of 3D dynamic interaction of T cells (red dots) and DC monolayer (green monolayer) from real 3D confocal visualization, using Bitplane Imaris (yellow arrows indicate flow direction). Scale bars: **a)** 1cm; **b)** 1 mm; **d)** 10 µm.

Dendritic cells: Dendritic cells were loaded onto device and let adhere to fibronectin coating for 20 min and preincubated with 100 ng/ml LPS for 2h. After 2h, the cells were incubated with the ovalbumin OVA323-339 I-Ab-(MHC class II)-presented peptide (ISQAVHAAHAEINEAGR) (here after called OVAII peptide) or the OVA257-64 Kb (MHC class I)-presented peptide (SIINFEKL) (here after called OVAI peptide), both at 10 µg/ml and 100 ng/ml lipopolysaccharide (LPS, Sigma) for 1 h, for antigen presentation to or CD4+ or CD8+ T cells, respectively.

Staining cells: Cells were removed from flasks and stained with 1 µM Cell TrackerTM Deep Red Dye or 5 µM Cell TrackerTM Orange CMTMR (5-(and-6)-(((4-chloromethyl)benzoyl)amino) tetramethylrhodamine (Invitrogen) for 30 minutes according to protocols and re-suspended to a final concentration of ~5x10^{6} cells/ml.

Microfluidic setup: The cells were imaged in a Zeiss LSM 510 inverted confocal microscope, which was equipped with an on-stage incubator with controlled temperature, CO_2 pressure and humidity for long term cell tracking. Microscope and

digital camera were controlled via Carl Zeiss Zen 2009 (Version 6.0 SP2). Syringe pumps (PHD 2000, Harvard Apparatus, Holliston, MA) were used to insert cells and fluids into the microfluidic structure [Fig. 1(a) (b) (c)]. T cells:DCs interactions were visualized in 2D and 3D at different times, using a fully rendered multidimensional dataset and a scheme of monochrome z-stacks, resulting in a "top view" projection. Time lapse fluorescence and differential interference contrast (DIC) images were captured using a 20x objective while maintaining devices at 37˚C using Zeiss LSM 510 inverted laser scanning confocal microscope. The fluorescence micrographs were analysed on Matlab R2014, Bitplane Imaris 7.6 and ImageJ software. Cells were manually tracked over time from maximum intensity top-view image sequences. Instantaneous velocity of T cells and DC were calculated from the distance moved between successive time points (~ sec each).

F. Mechanical strength assay of pMHC-TCR

The microfluidic system described above was used in this work to measure the detachment of cells at certain tangential force via controlled shear stress threshold of pMHC-TCR binding for specific and non-specific antigen activation for $CD4^+$ T cells and $CD8^+$ T cells. In order to generate stimulation, $CD4^+$ MF2.2D9 T cell and $CD8^+$ RF33.70 T cell recognising OVAII/I-A^b and OVAI/K^b, respectively. In this way to promote these interactions, one uniform DC monolayer activated or not with LPS and OVA II or I peptide was prepared, and $CD4^+$ or $CD8^+$ T cells were loaded by pipetting from the inlet of the microchannel [Figure 1(b)]. To allow formation and strengthen these interactions, the microchannel co-culture was incubated at 37˚C for 30 min. The microchip was then mounted on confocal and connected with the syringe pump. For these cell detachment assays, the flow rate was increased every 20 min (from 100 nL/min to 1000 µL/min) to probe the shear stress in five orders of magnitude (from 0.01 to 100 Dyn.cm^{-2}). The number of cell-cell interaction was determined by time-lapse microscopy in two different positions in the same channel and plotted as a function of shear stress. In this approach, the same experimental setup was used to investigate the cell rolling and the cell tracing, when these interactions are subjected to an increase of shear stress.

G. Adhesion cell assay for interaction of T cells:DCs

To probe the dynamics of cell attachment, T cells were introduced into the microchannel by continuous flow, as opposed to the static no-flow establishment of cell:cell adhesion in protocol F. A microchannel with a uniform DC monolayer with and without activation with LPS and OVA II peptide (or OVA I peptide), was connected to the syringe pumps with $CD4^+$ T cells and $CD8^+$ T cells and the T cells loading was performed at 0.01 Dyn.cm^{-2} for 80 minutes of continuous perfusion on the two inlets, allowing the presence of two parallel flow streams with the two different T-cell lines along the microchannel. Then, both cell syringes were replaced by medium syringes starting the detachment approach: the flow rate was increased 10-fold every 10 min (from 100 nL/min to 1 mL/min) to probe the corresponding to wall shear stress in from 0.01 to 100 Dyn.cm^{-2}. In this context, this experimental approach was used to investigate the model of cell-cell interaction, the cell surface distribution, the cell rolling and cell tracing at an increasing shear stress.

H. Statistical analysis

Measurements of T cell:DC interaction and DC monolayer were obtained and quantified using time series (Zeiss LSM510) across 12 independent experiments, at two separate locations, 4 mm and 7 mm from the beginning of the initial bifurcation of the microchannel. Considering that the results obtained in both positions were similar in all experiments, we opted to mention just one position, 7 mm, to simplify the description of this work. For the cell counting, any T cell interacting with DC that did not move for 30 s was considered adherent. For statistical clustering treatment, multiple stack samples along time were performed and compared in Matlab R2014, Bitplane Imaris 7.6 and ImageJ software, on the multidimensional data set assembled using custom written scripts to resolve cell count and stages of antigen recognition and $CD4^+$/$CD8^+$ T cells activation over time [Fig. 1(d)].

Results and Discussion

Simulations: Flow Configuration and Shear Stress Profile

In order to understand the progressive distribution of shear stress along a cross-section (XZ) at any position (Y) of the rectangular microchannel and for the different flow rates that were experimentally applied, a set of simulations were performed in COMSOL Multiphysics 4.4. In this context, biomimetic microfluidic systems are particularly suited for studies of cell-adhesion and cell-cell interaction dynamics during variable velocity, shear stress, deformation rates and migratory motility. The shear stress of interest in this study relates to the conditions found during an inflammation process, characterized by an increment of shear stress inside the T cell zones of LNs during the stage II (3), where in the presence of cognate antigen, T cells arbitrarily migrate along the fibroblastic reticular cell (FRC) conduit networks to contact the cognate antigen present by surrounding APCs. During this stage, T cell speed decreases and increases turning behaviour (stop signal), occurring serial contacts with multiple DCs during 2 h (2, 3, 32, 34-36, 38, 39, 44). Assuming the complexity of estimating the hydrodynamic properties in the highly confined microenvironment of T cells zones inside LNs, several studies that focused on the microvasculature suggest that the shear stress tested can be representative on the range of interstitial flow velocity measured in normal and tumor-associated inflamed skin, with a range 0.005 to 0.05 Dyn.cm^{-2} (37).

As a result, in Figure 2(a) we can observe that the shear stress is negligent in the centre of the channel and increases when reaching the edges of the channel, where the cells are immobilized and interacting. From the model, we found the shear stress values for the different flow rates used in our system (Figure 2(a) (b)) at the positions (X, Y, Z) of (A) the DC monolayer (500,Y,5)), (B) the center of the channel (500,Y,50), (C) representative region on the top of the T cell experiencing

higher work (750,Y,15) and (D) the representative region of a detached T cells (750,Y,25).

In this way, it is possible to adjust the extrinsic shear force to the intrinsic inter-cell force of cell:cell adhesion to mimic lymph node conditions and to promote selective binding of antigen-specific vs non-specific T cells to the DC monolayer. At low shear stress (0.01 to 0.05 Dyn.cm^{-2}, associated with flow rates ranging from 100 nL.min^{-1} to 500 nL.min^{-1}) (37) corresponding to physiological values for complex flow in the lymph node microenvironment (15, 45, 46) yielded cell speeds of 8-25 µm per second, so cells have about 1 second to establish firm contact with another cell.

On a second phase, these established T cell:DC interactions were submitted to a successive increment of shear stress values (from 0.01 to 100 Dyn.cm^{-2}) to determine the mechanical strength of the cell:cell interaction and the suitable speeds for differentially braking the bond of antigen-specific *vs* non-specific interactions (4, 10, 13, 47). We assessed the activation of DCs showing expression of MHC class II and CD80/86 by flow cytometry (data not shown).

Our objective in this work was to explore the mechanism, dynamics and basic cell behaviour of attachment and detachment of antigen-specific and unspecific CD8$^+$ T cells and CD4$^+$ T cells to activated antigen-presenting or non-activated DCs during flow at different shear stresses to establish some basic principles and approaches to allow further exploration of these phenomena.

In T cell:DC interactions, when an antigen is present, the initiating interaction leads to a highly organized structure of the immunological synapse known as the central, peripheral and distal supramolecular activation complexes (SMACs). The formation of SMAC is dependent on mechanical force, cell-cell contact area and time, shear stress, expression of surface molecules (such as TCR and LFA-1), cytoskeleton dynamics, antigen affinities and cell phenotype. In this work, our objective was to first allow establishment these interactions with low shear stress before successive increment of flow rates mimicking the evolution of inflammatory stages.

The process of attachment starts within seconds after conjugation and reaches a maximum strength at around 30min before cell activity causes changes in adhesion and subsequent release (18). In this sense, we find it likely that T cells interact with DCs in a history dependent manner where in particular the detachment is dynamic and reliant on previous encounters, making it likely that other flow-change regimes would change cell behaviour. In this work we sought however to find the working limits of our system, and more work is needed to fully understand the mechanisms of attachment and release.

Characterization of adhesion DC monolayer and T cell:DC interactions under 0.01 Dyn.cm^{-2}

The interaction of dendritic cells to adsorbed films of fibronectin (FN) and collagen (Col) was optimized showing that after 1 h on FN-coated surface, DCs spread uniformly along the microchannel, with a characteristic morphology with long dendrites and a larger surface area, in accordance with

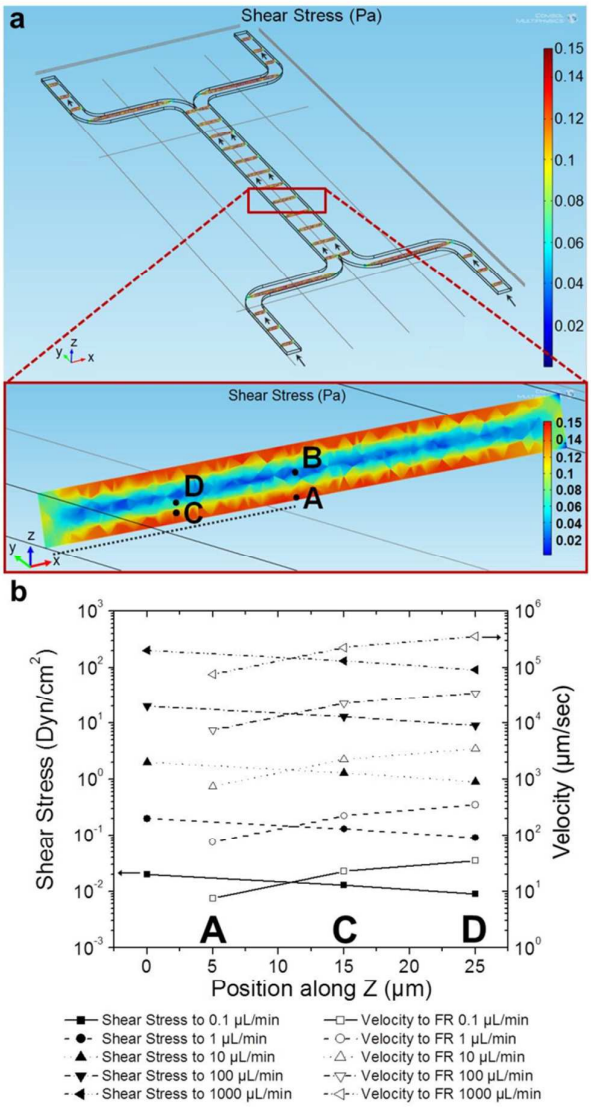

Figure 2| Shear Stress Profile a) 2D graphics from COMSOL Multiphysics 4.4 simulation of a rectangular channel cross section. **b)** Shear stress in a rectangular channel cross section as a function of different positions along Z axis at different flow rates (µL/min).

expected morphology and overall function. In contrast, on Col coated microchannels DCs were poorly dispersed and with thinner and shorter dendrites, similarly to what is observed on uncoated glass. All subsequent experiments were therefore done in FN-coated channels, as ECM components have shown beneficial effect on DC function (8, 9, 48-50). Our findings of a positive effect of FN coating on DC surface area and dendritic length are in line with these studies (8, 9, 48).

The DCs normally found in lymph nodes having migrated from peripheral tissues and able to prime T cells, are proinflammatory expressing co-stimulatory molecules and secrete cytokines and chemokines. We activated the DCs with LPS for a total of 3 h after the initial DC loading and adherence. The DC monolayer acquired a mature phenotype, increasing in

size presumably as a part of a strategy to increase the probability of encounters with naive antigen specific T cells.

To better understand the intercell dynamics, we co-incubated OVAII-peptide specific MHC class II-restricted $CD4^+$ T cells on LPS-activated OVAII-peptide presenting DCs for 30 min before starting the perfusion at 0.01 $Dyn.cm^{-2}$ for 2 h, a shear stress representative of the interstitial tissue flow velocity (37). By tracking single cells over time, the trajectories of $CD4^+$ T cells could be established. During the initial 30 min with perfusion, the interactions had a mean duration of 12.8 min, the mean velocity of T cells was 6.0 $\mu m.min^{-1}$ (n=422 cells), and most of the T cells crawled around making dynamic serial contacts with the same or with neighbouring DCs (Figure 3 and Videos (S1)). This cell behaviour is very similar to what is found *in vivo* (3, 37). In fact, Miller *et al.* reported that *in vivo* the interactions were prolonged in the presence of antigen with the mean-time of 11.4 min, and remained intermittent with a mean-velocity of 5.4 $\mu m.min^{-1}$ (3).

We also observed the tendency of $CD4^+$ T cells to move against the direction of flow (Supplementary figure 1, S1 Movie), as also reported in (38), even though the collective analysis showed more or less random movement, independent of flow direction (3). This discrepancy can be explained by that our DCs are not completely confluent, which introduces gaps in the contra-flow crawling substrate not present in monolayers of ICAM-1-Fc, that the density of ICAM-1 on the DC surface probably is lower than on the ICAM-1-Fc covered surface, and that T cells and DCs interact dynamically to influence each other's behaviour compared to the mono-cell behaviour reported by Valignat *et. al.* (38).

DC:T cell interactions at Low Shear Stress Variations

To further characterize the T cell:DC interactions and asses the longevity and strength of the contacts, we allowed $CD4^+$ and $CD8^+$ T cells to adhere to activated antigen-presenting or control DCs for 30 min as previously, at physiological shear stress ranging from 0.01 to 0.15 $Dyn.cm^{-2}$ increasing every 20 minutes for a total of 4h.

The magnitude of the shear stress in Figure 4(b) is lower compared to Figure 4(a) for the same flow rates since T cell positions are farther from the surface (as evidenced in Figure 2), which decreases the shear stress. In conjugation with the model presented in Figure 2, these specific positions (A, C, D in Figure 2) along the cross section of the channel for the different flow rates used in our system were selected to estimate the specific value of shear stress applied on specific cell positon: Figure 4(b) describes the magnitude of shear stress in the region of a T-cell interacting with a DC monolayer (position C (750,Y,15) Figure 2), and Figure 4(a) represents the shear stress that dendritic cells (position A (500, Y, 5) Figure 2) are submitted to.

There was a successive decrease in the number of DC adhesion to FN-layer and activated DCs adhered more firmly to the fibronectin substrate than unactivated cells (Figure 4 (a)).

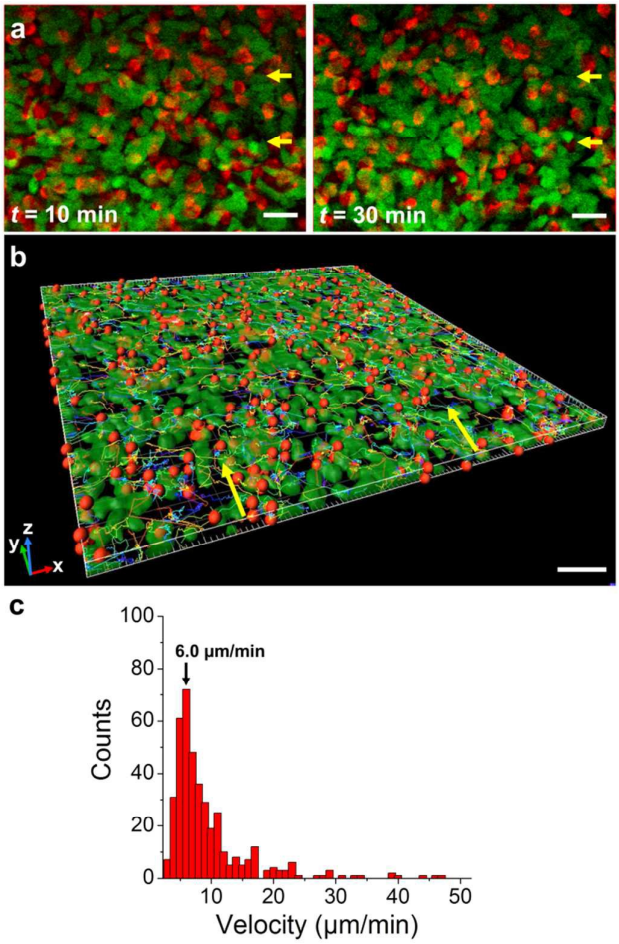

Figure 3| Dynamic cognate T cells:DCs interactions. a) Time-lapse images of cognate interactions between T cells (red) with APCs (green) during 30 min were examined by confocal microscopy. Yellow arrows indicate the direction of flow. **b)** Three-dimensional model of interactions T cells (red dots) and APC monolayer (green monolayer) using ImarisTrack. **c)** Distributions of instantaneous CD4+ T cells velocities, measured during 30 min at times of 0-2h (n=422 cells) restricted to 35 µm from the surface. Scale bars: **a)** 15 µm; **b)** 50 µm.

We also observed that the morphology of the DC changed to an elongated shape, with enlarged contact area to the FN-substrate thus resulting in higher adhesive properties (10, 25, 51).

The number of T cell:DC interactions also decreased along time with increase of shear stress, but showing a much slower detachment rate from LPS-activated antigen-loaded DCs compared to the control DCs (Figure 4 (b)). The overall half-life of $CD4^+$ T cell contact to control DC was in the order of 75 min, whereas the half-life of the interaction with activated antigen-loaded DCs was more than 4 h indicating that activation and antigen provided more stable conjugation of the cell pairs.

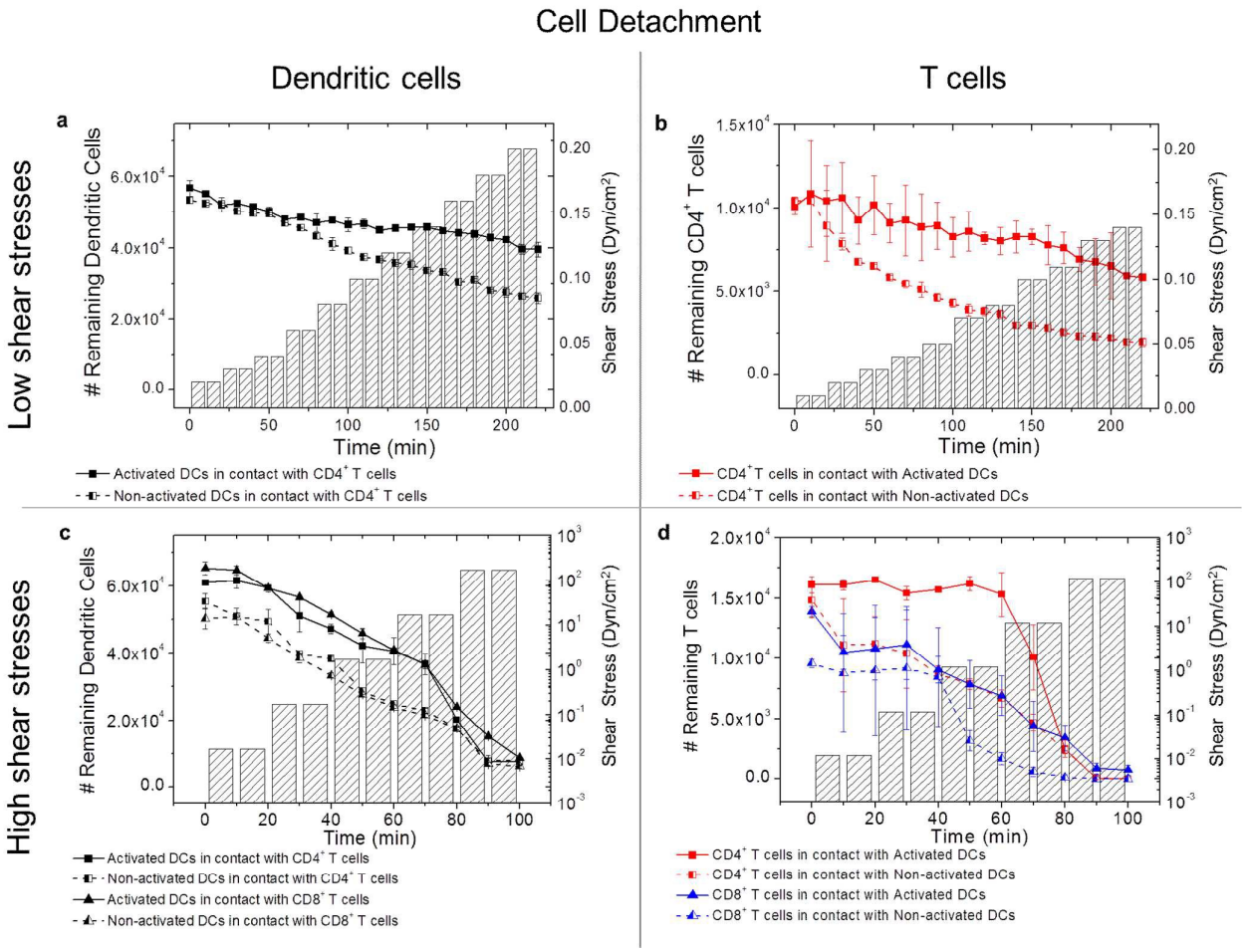

Figure 4| T cells:DCs interactions based on bond affinity and number: experimental distributions of high and low affinity bonds associated respectively with and without activation with LPS and OVA II peptide, increasing the velocity in 20 min: Low shear stress variations: Detachment of **a)** dendritic cells and **b)** T cells; High shear stress variations: Detachment of **c)** dendritic cells and **d)** T cells.

The cross-talk of T cell:DC involves several receptor-ligand interactions (as co-stimulatory and adhesion molecules), and the delivery of soluble mediators responsible to modulate the outcome of T cell activation, as clonal expansion and differentiation (6). The sustained adhesion of $CD4^+$ T cells to DCs at progressive increase of shear stress could be explained by two possible regulation mechanisms (10, 49, 52): (i) the integrin activation step on T cells allowing a stable leukocyte adhesion and, (ii) the presence of high density of specific contacts of pMHC at the surface of APCs.

When T cells roll over the DC monolayer, and when the recognition is established by TCR binding to peptide-MHC of APC, the TCR triggers a signalling cascade. Others have established that mechanical forces are involved in discriminating endogenous from foreign pMHC and on activation of TCR triggering, described in several studies via traction force microscopy (TFM), atomic-force microscopy (AFM), optical tweezers (OT) and biomembrane force probe (BFP) (4, 13, 18, 46, 53-55). Reinherz *et al.* describes the importance of tangential but not perpendicular mechanical force on the TCR complex activation, evidencing the need for force during the activation, and by this defining the TCR as an anisotropic mechanosensor (46, 54). Once established the TCR-peptide MHC interactions will resist of shearing forces (46, 47). Reinherz *et al.* presents as main implications associated by this directional-specific physical force that (i) TCR activation may be promoted due to the torque application, the angle of interaction between the pMHC-TCR lever arm length and force vector will affect the torque (15); (ii) shear stress can promote catch bonds at the TCR-pMHC interface, which are strengthened by tensile force, improving binding and ligand specificity; (iii) the total force exerted to the T cell surface is defined by movement of the T cell membrane relative to the T cell:APC contact zone and the sensitivity is built into TCR mechanosensor function (45, 46). Thus a low shear force promoted antigen-specific T cell adhesion to DCs.

DC:T cell interactions at High Shear Stress Variations

We next sought to determine the threshold shear stress necessary to break the inter-cell conjugation at shear stress

values found inside capillary venules (0.01-1 Dyn.cm^{-2}) and inside arteria (>50 Dyn.cm^{-2}) (9, 38).

For the same reasons mentioned above, the magnitude of the shear stress represented in Figure 4(d) is lower compared to 4(c) because the T cells are assumed to be farther from the surface than DC monolayer, decreasing in this way the shear stress they are submitted to.

The DCs detached from the FN-layer with a steady rate with no clear threshold level for shear stress (Figure 4(c)). There was a tendency that activated DCs adhered more firmly to the substrate than non-activated, particularly at intermediate shear stresses. There was no influence of the presence of CD4+ or CD8+ T cells on the detachment rate of DCs. Having established the background instability of the DC layer, we next assessed the detachment of CD8$^+$ and CD4$^+$ T cells from activated antigen-loaded and from control DCs.

The number of CD4$^+$ T cells conjugated to DCs was fairly stable at low shear stress, but dropped abruptly above 12 Dyn.cm^{-2} (Figure 4(d)). The number of CD4$^+$ T cells adhering to peptide-presenting DCs after the initial rinse (i.e. after 10 min of perfusion) was significantly higher than to non-activated DCs, and the difference remained high until a threshold shear stress of 12 Dyn.cm^{-2} was reached, when all T cells were released. Also the cytotoxic CD8$^+$ T cells showed a higher affinity to peptide-presenting DCs than to non-activated DCs, even though these interactions were a lot less stable and were steadily decreasing also at lower shear stresses. These observations show clearly that CD4$^+$ T cells have a strong interactions with the activated peptide-loaded APCs and therefore, we can infer that this activation was antigen-specific and that our system possibly can be used to selectively affinity isolate antigen-specific T cells and be used as microphysiological system of partial lymph node functionality.

The cell:cell interaction is dependent on the formation of SMAC, where a major contribution comes from ICAM-1 – LFA-1 binding. This binding is again dependent on signalling through TCR, on mechanical force exerted on the ICAM-1 – LFA-1 bond and on the expression level, type and stability of the ICAM-1 and LFA-1 molecules. The observed difference between CD8$^+$ and CD4$^+$ T cell release force can be due to generally higher antigen-specific activation, determined by cytokine release, in this particular MF2.2D9 CD4$^+$ T cell clone compared to this particular RF33.70 CD8$^+$ T cell clone (data not shown). A further explanation can be that the MHC-level in MD2.2D9 is considerably higher than in the RF33.70 (data not shown), which should result in higher antigen-specific activation of the CD4$^+$ T cells. These release force numbers will probably vary much between different clones and cell pairs, but will also probably lie within our reported ranges.

To account for the steady decrease in DC from the channel as well as to evaluate the efficiency in the formation and the stability of T cell:DC conjugates, we further analysed the relative T cell to DC ratios for different times and shear stresses. In our system, there was about one T cell for every five DC initially. At low shear stresses this ratio remained fairly constant over time for the interaction of CD4$^+$ T cells with activated peptide-loaded DCs (Figure 5(a)), even though the number of DCs adherent to the fibronectin slowly decreased (Figure 4(a)). This means that the adhesion of DCs to the substrate was neither strengthened nor weakened by conjugation to CD4$^+$ T cells. The ratio of CD4$^+$ T cells to resting DCs decreased to half of the initial ratio, suggesting that the binding strength in the conjugate was lower than the adherence of DC to the substrate. This difference can be exploited to selectively retain antigen–specific T cells to a cognate activated DC. At higher shear stresses, the ratio of CD4$^+$ T cells to DCs was stable until the threshold shear stress around 1.2 Dyn.cm^{-2}, whereafter both DCs, T cells and conjugates released from the channel substrate (Fig 5b). However, there was higher ratio of T cells to activated Ag-loaded DCs than to resting DCs, suggesting higher binding forces. Considering that the high depletion of CD4$^+$ T cells occurs at 12 Dyn.cm^{-2} and assuming the case of the flow past a sphere at low Reynolds numbers (Re<<1), we can estimate the total drag force (F_D) on the T cell as a grand resultant force from pressure force and viscous shear stresses on the cell, known as Stokes' law $F_D=6\pi\mu vR$. In this case, considering the variation range of flow rates tested in this system during time associated to (0.0023<Re<2.6) and the restrictions of Stokes' law to Re<0.1, the expression for the drag force $F_D=6\pi\mu vR$, needs to be improved with additional method of matched asymptotic expansions as referred by (56), leading to the derivation of Oseen's correction ($F_D=6\pi\mu vR[1+(3/8)Re]$) and being valid for Re up to ~1. Assuming μ as dynamic fluid viscosity (for culture medium at 37°C) 0.72x10-2 N.s/m^2, R the radius of the T cells (5 µm) and v the fluid velocity (i.e., at velocity 0.033 m/s associated to Re 2.6, when occurs depletion of CD4$^+$ T cells at 12 Dyn.cm^{-2}) (56), and we can estimate that a force of ~4.8 nN was applied to the T cells. The cell interaction dynamics in the CTL CD8$^+$ T cells systems was different, showing antigen-specific retention above 1.2 Dyn.cm^{-2}. From this we can estimate that for these cell lines the resultant force applied in the detachment of CD4$^+$ T cells on activated DCs is around ~4.8 nN, and for CD8$^+$ T cells on non-activated system is around ~0.25 nN.

The antigen-specific T cell:DC interaction is strengthened by recruitment of LFA-1/ICAM-1 adhesion molecules to the immune synapse area. Shear stress on its own seems to have little influence on the adhesion molecule LFA-1, however the chemokines CCL19 and CCL21 have an important influence on the upregulating the active form of LFA-1 on DCs (57), as well as the binding of TCR to pMHC (18). LFA-1 then binds ICAM-1 on the T cells forming the immunological synapse, which seems to be strongest after 30 min and is stable for 1-2 h (18, 49, 52).

Several groups have provided evidence about the mechanical force of the interaction between T cells and APC (18, 38, 58). Hosseini *at el.* with single-cell force spectroscopy by AFM measured of long-time interaction forces between T cells and APCs, and demonstrated in the presence of antigen interaction forces increased from 1 to 2 nN at early points, achieving at 30 min a maximum of interaction force of ~14 nN, and decreasing the interaction forces after prolonged contact time (>60min) (18, 58). Valignat *et al.* investigated how migrational speed and

directionality of T lymphocytes are influenced by variations of shear stress from 2 to 60 Dyn.cm^{-2}, demonstrating that the force imposed by fluid flow in individual cells was estimated around ~0.6 nN, corresponding to a shear stress 60 Dyn.cm^{-2} exerted on a typical cell surface (38). The result obtained in this work match the interval of forces obtained by Hosseini *et al.* and Valignat *et al*. APCs, and demonstrated in the presence of antigen interaction forces increased from 1 to 2 nN at early points, achieving at 30 min a maximum of interaction force of ~14 nN, and decreasing the interaction forces after prolonged contact time (>60min) (18, 58). Valignat *et al.* investigated how migrational speed and directionality of T lymphocytes are influenced by variations of shear stress from 2 to 60 Dyn.cm^{-2}, demonstrating that the force imposed by fluid flow in individual cells was estimated around ~0.6 nN, corresponding to a shear stress 60 Dyn.cm^{-2} exerted on a typical cell surface (38). The result obtained in this work match the interval of forces obtained by Hosseini *et al.* and Valignat *et al*.

Our observed differences in the intercell dynamics of CD8$^+$ and CD4$^+$ T cells to DCs, where the CD4$^+$ cell interaction with DC seemed to be longer and more stable than the relatively more transient CD8$^+$ T cell:DC interaction, which is in line with other publications (3). This fact suggests that this heterogeneity is part of a normal immune response and an important role in diversifying T cell fate (6, 59).

The detachment of T cell:DC contacts is also influenced by the strength of TCR signalling, the number of TCR-MHC interactions, and as a response to neighbouring chemokine environment, resulting in segregation and redistribution of established CD4$^+$ T cell:DC conjugates (47, 51, 52).

It is also important to note that there is a major difference in shear stress experienced by DCs at 5µm and T cells at 15µm from surface, as shown by retention of 70 % and 40 % at 20 Dyn.cm^{-2} for activated and non-activated DCs, respectively (Figure 4(c) and Figure 6), whereas only 10% of T cells remained after 10 Dyn.cm^{-2} for 20 minutes (Figure 4(d)). Thus, the force of binding of DCs to FN is much stronger and lasting than T cells binding to DCs, as may be representative of forces inside lymph node conduits where DCs line the hollow tubes and T cells are in the center flow in between (2, 10, 51).

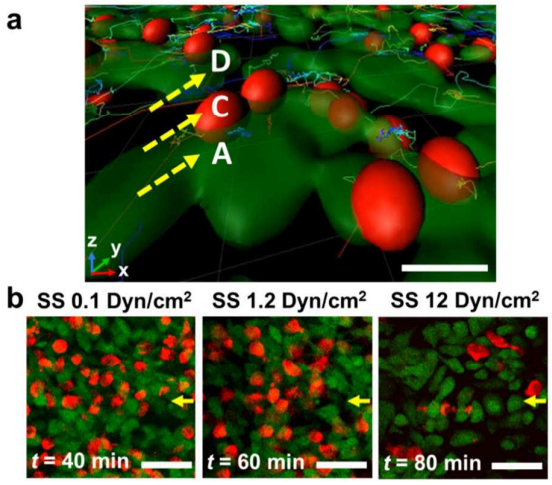

Figure 6| Applying high shear stress variations between CD4$^+$ T cells with APCs: a) Shear stress in function of different positions (A, C and D) along Z axis in a channel cross section, as illustrated in Figure 2. **b)** Evolution of cell adhesion strength over time. Scale bars: **a)** 10 µm; **b)** 15 µm.

Adhesion cell model for specific interaction of T cells:DCs

Having established the influence of shear stress on the dynamic behaviour of the conjugates at different flow rates, we next wanted to establish the dynamics and rate of attachment of T cells to activated antigen-loaded DCs in a continuous flow, rather than by a preceding static synapse-forming stage. In this approach, the T cell:DC interaction is not forced, but allows for a degree of freedom of orientation to establish contact, due to the tangential mechanical force applied over time by the flow. We also exploited the laminar flow in microfluidic devices by applying two different streamlines, one with CD4$^+$ T cells and one with CD8$^+$ T cells over a common DC monolayer previously activated with either LPS+OVA II peptide, LPS+OVA I peptide or untouched DCs at a low flow rate determined from previous experiments. We found a much higher degree of antigen-specific adhesion using this approach (Figure 7) than the detachment approach. For the activated DC monolayer preincubated with LPS+OVA II peptide for 80 min and applying low shear stress (0.01 Dyn.cm^{-2}), we found highly specific adhesion of antigen-specific CD4$^+$ T cells compared to the non-specific CD8$^+$ T cells (Figure 7(a)). The number of CD4$^+$ T cells interactions was approximately constant over time with (~6.4x10^3) CD4$^+$ T cells to (~6.0x10^4) APCs, reflecting an interaction ratio of 11% compared to virtually no binding of CD8$^+$ T cells. After the initial 80 min attachment, the flow was switched to medium and subjected to increasing flow rates every 10 minutes. As shown in Figure 7(a), we observed a successive detachment of CD4$^+$ T cells with a successive increment of shear stress from 0.01 to 12.0 Dyn.cm^{-2}, and a strong decrease when increasing the shear stress to 120.0 Dyn.cm^{-2}. On the other hand, the non-specific interaction of CD8$^+$ T cells were only broken when submitted to a high shear stress in the range 12.0-120.0 Dyn.cm^{-2}.

This subsequent detachment was similar to what we found in the statically attached T cells (Figure 4 and Figure 5), with depletion of CD4$^+$ T cells occurring from 12 Dyn.cm^{-2} and associated with a force of 4.8 nN. In this context, this attachment approach provides a simple way to control the natural formation of T cell:DC contact similar to in vivo, with an interaction ratio of T cells vs APCs of 11% comparing to the 33% (~2.0x10^4 CD4$^+$ T cells per ~6.0x10^4 APCs) of the detachment approach. These results also show that the lower quantity of interactions in this attachment approach can be explained by the fact that the total number to T cells interacting on DC monolayer was lower and dependent on the balance between the convection velocity and sedimentation velocity that promotes cell rolling, adhesion and posterior interaction.

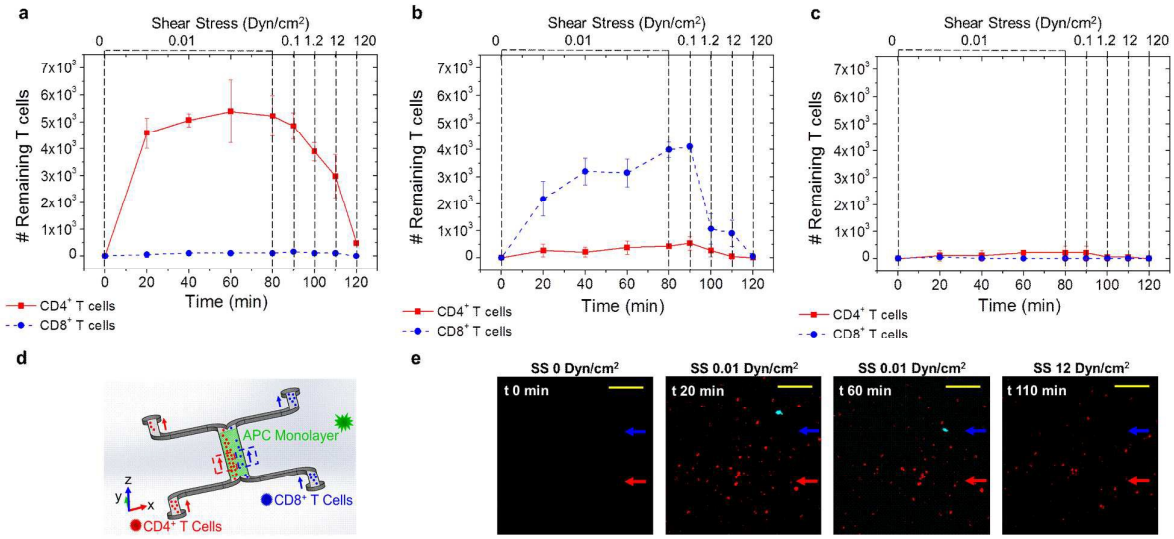

Figure 7| Antigen specific attachment and shear stress induced detachment under continuous flow. $CD4^+$ T cells and $CD8^+$ T cells were continuously loaded by perfusion from the two inlets for 80 min with 0.01 Dyn.cm^{-2} into previously activated and antigen-loaded DC microchannel allowing the presence of two parallel flow streams with two types of T-cells in parallel. After 80 min cell perfusion was stopped and replaced with pure medium increasing the flow rate 10-fold every 10 min (from 100 nL/min until 1 mL/min) corresponding to wall shear stress from 0.01 to 100 Dyn.cm^{-2}. **a)** Antigen-specific interactions of $CD4^+$ T cells with OVA II loaded DCs *vs.* antigen-unspecific $CD8^+$ cells. **b)** Antigen-specific interactions of $CD8^+$ T cells with OVA I loaded DCs *vs.* antigen-unspecific $CD4^+$ cells. **c)** Antigen-independent attachment of $CD8^+$ and $CD4^+$ T cells to antigen-free DCs. **d)** Schematic illustration of the cell-loading and pairing protocol. The main channel is coated with a monolayer of adherent DCs (in green). The direction of the flow of $CD8^+$ and $CD4^+$ T cells is indicated, respectively by red and blue arrows. **e)** Representative images used for analyses of cell attachment of $CD4^+$ T cells (red) and $CD8^+$ T cells (cyan) to DCs for 60 min with 0.01 Dyn.cm^{-2} (attachment phase) and 110 min with 12 Dyn.cm^{-2} (detachment phase). Scale bars: **c)** 50 µm.

According to Bousso P. *et al.*, in the absence of antigen recognition, $CD8^+$ T cells may tend to encounter DCs that have already established a cognate interaction with other $CD4^+$ T cell, as an eventual result of chemokine expression and production (CCL3 and CCL4) (6). This fact may explain the reason why some CD8+ T cells bound non-specifically to the DCs.

Also in the reverse condition (Figure 7(b)), $CD8^+$ cells selectively bound to Ag-loaded DCs, whereas few $CD4^+$ cells nonspecifically bound. During 80 min with the same shear stress (0.01 Dyn.cm^{-2}), the number of $CD8^+$ T cells that interacted during this approach, was around (~4.0x10^3) T cells to (~6.0x10^4) APCs, meaning an interaction ratio of ~7%. In the subsequent detachment, we observed an early depletion of specific $CD8^+$ T cells at 1.2 Dyn.cm^{-2}, and a successive detachment with increasing shear stress 0.12-12 Dyn.cm^{-2}, with no cells remaining at 120 Dyn.cm^{-2}.

This attachment approach can be assumed as a complementary method of the initial detachment approach. This allows the confirmation of cell detachment behaviour and the shear stress applied to detach the cells in both approaches and highlights the existence of the heterogeneity response as a part of a normal immune response and important role in diversifying T cell fate (6).

Conclusion

During T cell priming and activation, a few antigen-presenting dendritic cells residing in lymph node interact with a large number of T cells entering the lymph node from the blood, scanning for match in TCR with peptide on MHC molecules on the DCs.

In this work we have explored the mechanism, dynamics and basic cell behaviour of attachment and detachment of antigen-specific and unspecific $CD8^+$ cytotoxic T cells and $CD4^+$ T helper cells to activated or non-activated DCs during flow at different shear stresses. The main goal of this study was to investigate the interaction induced by tangential force via shear stress from natural dynamic rate of attachment of T cells:DC in a continuous flow, as a way to mimic the natural principle of interaction that occurs *in vivo* and to investigate the possibility to use these principles as tools towards immunological research and in development of novel immunotherapeutic approaches.

We successfully demonstrated the ability of our system to selectively promote adhesion of antigen-specific T cells through serial contacts. Furthermore, we found antigen-specific attachment and detachment at different shear stresses, suggesting that a shear stress of 0.1-1 Dyn.cm^{-2} can be used to allow cell-based affinity-isolation of antigen specific T cells towards unknown antigens.

In contrast to static cultures or passive channels our system can be used to compare, in parallel and in real time, through control over adhesion, the effect of different treatments, inhibitors, activators or immunogens. The applications can be as a research tool to understand lymph node organogenesis, T cell development and activation, contribution of different cell

types in immunization protocols, generation of specific immune responses and as a clinical developmental tool towards *in vitro* immunization, personalized cancer vaccination, immunotherapeutic approaches for cancer and autoimmune diseases etc., all through re-creation of the natural T cell activation lymph node organ. Further investigations are needed to verify the feasibility of the approach at a clinical scale.

Acknowledgement

The Research Council of Norway is acknowledged for the support to the Norwegian Micro- and Nano- Fabrication Facility, NorFab (197411/V30). Microfabrication process was performed at the NTNU NanoLab (NorFab), Norwegian University of Science and Technology. Experiments were performed at the Cellular and Molecular Imaging Core Facility (CMIC), Norwegian University of Science and Technology. CMIC is funded by the Faculty of Medicine at NTNU and Central Norway Regional Health Authority.

References

1. Swartz MA, Hirosue S, Hubbell JA. Engineering approaches to immunotherapy. Science translational medicine. 2012;4(148):148rv9.
2. Girard JP, Moussion C, Forster R. HEVs, lymphatics and homeostatic immune cell trafficking in lymph nodes. Nature reviews Immunology. 2012;12(11):762-73.
3. Miller MJ, Safrina O, Parker I, Cahalan MD. Imaging the single cell dynamics of CD4+ T cell activation by dendritic cells in lymph nodes. The Journal of experimental medicine. 2004;200(7):847-56.
4. Ma Z, Discher DE, Finkel TH. Mechanical force in T cell receptor signal initiation. Frontiers in immunology. 2012;3:217.
5. Mirsky HP, Miller MJ, Linderman JJ, Kirschner DE. Systems biology approaches for understanding cellular mechanisms of immunity in lymph nodes during infection. Journal of theoretical biology. 2011;287:160-70.
6. Bousso P. T-cell activation by dendritic cells in the lymph node: lessons from the movies. Nature reviews Immunology. 2008;8(9):675-84.
7. Miller MJ, Wei SH, Parker I, Cahalan MD. Two-photon imaging of lymphocyte motility and antigen response in intact lymph node. Science. 2002;296(5574):1869-73.
8. Garcia-Nieto S, Johal RK, Shakesheff KM, Emara M, Royer PJ, Chau DY, et al. Laminin and fibronectin treatment leads to generation of dendritic cells with superior endocytic capacity. PloS one. 2010;5(4):e10123.
9. Young EW, Wheeler AR, Simmons CA. Matrix-dependent adhesion of vascular and valvular endothelial cells in microfluidic channels. Lab on a chip. 2007;7(12):1759-66.
10. Bianchi E, Molteni R, Pardi R, Dubini G. Microfluidics for in vitro biomimetic shear stress-dependent leukocyte adhesion assays. Journal of biomechanics. 2013;46(2):276-83.
11. van der Merwe PA. The TCR triggering puzzle. Immunity. 2001;14(6):665-8.
12. Ma Z, Finkel TH. T cell receptor triggering by force. Trends in immunology. 2010;31(1):1-6.
13. Li YC, Chen BM, Wu PC, Cheng TL, Kao LS, Tao MH, et al. Cutting Edge: Mechanical Forces Acting on T Cells Immobilized via the TCR Complex Can Trigger TCR Signaling. Journal of immunology. 2010;184(11):5959-63.
14. Grakoui A, Bromley SK, Sumen C, Davis MM, Shaw AS, Allen PM, et al. Pillars article: The immunological synapse: a molecular machine controlling T cell activation. Science. 1999. 285: 221-227. Journal of immunology. 2015;194(9):4066-72.
15. Kim ST, Shin Y, Brazin K, Mallis RJ, Sun ZY, Wagner G, et al. TCR Mechanobiology: Torques and Tunable Structures Linked to Early T Cell Signaling. Frontiers in immunology. 2012;3:76.
16. Martinez-Rico C, Pincet F, Perez E, Thiery JP, Shimizu K, Takai Y, et al. Separation force measurements reveal different types of modulation of E-cadherin-based adhesion by nectin-1 and -3. The Journal of biological chemistry. 2005;280(6):4753-60.
17. Zhang X, Wojcikiewicz EP, Moy VT. Dynamic adhesion of T lymphocytes to endothelial cells revealed by atomic force microscopy. Experimental biology and medicine. 2006;231(8):1306-12.
18. Hosseini BH, Louban I, Djandji D, Wabnitz GH, Deeg J, Bulbuc N, et al. Immune synapse formation determines interaction forces between T cells and antigen-presenting cells measured by atomic force microscopy. Proc Natl Acad Sci U S A. 2009;106(42):17852-7.
19. Muller DJ, Dufrene YF. Atomic force microscopy as a multifunctional molecular toolbox in nanobiotechnology. Nature nanotechnology. 2008;3(5):261-9.
20. Bhatia SN, Ingber DE. Microfluidic organs-on-chips. Nature biotechnology. 2014;32(8):760-72.
21. Khalili AA, Ahmad MR. A Review of Cell Adhesion Studies for Biomedical and Biological Applications. International journal of molecular sciences. 2015;16(8):18149-84.
22. Esch EW, Bahinski A, Huh D. Organs-on-chips at the frontiers of drug discovery. Nat Rev Drug Discov. 2015;14(4):248-60.
23. Huh D, Torisawa YS, Hamilton GA, Kim HJ, Ingber DE. Microengineered physiological biomimicry: organs-on-chips. Lab on a chip. 2012;12(12):2156-64.
24. Lamberti G, Prabhakarpandian B, Garson C, Smith A, Pant K, Wang B, et al. Bioinspired microfluidic assay for in vitro modeling of leukocyte-endothelium interactions. Analytical chemistry. 2014;86(16):8344-51.
25. Dong C, Lei XX. Biomechanics of cell rolling: shear flow, cell-surface adhesion, and cell deformability. Journal of biomechanics. 2000;33(1):35-43.
26. Kim SK, Moon WK, Park JY, Jung H. Inflammatory mimetic microfluidic chip by immobilization of cell adhesion molecules for T cell adhesion. The Analyst. 2012;137(17):4062-8.
27. Park JY, Kim HO, Kim KD, Kim SK, Lee SK, Jung H. Monitoring the status of T-cell activation in a microfluidic system. The Analyst. 2011;136(13):2831-6.
28. Choi Y, Hyun E, Seo J, Blundell C, Kim HC, Lee E, et al. A microengineered pathophysiological model of early-stage breast cancer. Lab on a chip. 2015;15(16):3350-7.
29. Faley S, Seale K, Hughey J, Schaffer DK, VanCompernolle S, McKinney B, et al. Microfluidic platform for real-time signaling analysis of multiple single T cells in parallel. Lab on a chip. 2008;8(10):1700-12.
30. Dura B, Voldman J. Spatially and temporally controlled immune cell interactions using microscale tools. Curr Opin Immunol. 2015;35:23-9.
31. Dura B, Dougan SK, Barisa M, Hoehl MM, Lo CT, Ploegh HL, et al. Profiling lymphocyte interactions at the single-cell level by microfluidic cell pairing. Nat Commun. 2015;6.
32. Bousso P, Robey E. Dynamics of CD8+ T cell priming by dendritic cells in intact lymph nodes. Nat Immunol. 2003;4(6):579-85.
33. Burbach BJ, Medeiros RB, Mueller KL, Shimizu Y. T-cell receptor signaling to integrins. Immunol Rev. 2007;218:65-81.

34. Henrickson SE, Mempel TR, Mazo IB, Liu B, Artyomov MN, Zheng H, et al. T cell sensing of antigen dose governs interactive behavior with dendritic cells and sets a threshold for T cell activation. Nat Immunol. 2008;9(3):282-91.
35. Hugues S, Fetler L, Bonifaz L, Helft J, Amblard F, Amigorena S. Distinct T cell dynamics in lymph nodes during the induction of tolerance and immunity. Nat Immunol. 2004;5(12):1235-42.
36. Miller MJ, Hejazi AS, Wei SH, Cahalan MD, Parker I. T cell repertoire scanning is promoted by dynamic dendritic cell behavior and random T cell motility in the lymph node. P Natl Acad Sci USA. 2004;101(4):998-1003.
37. Tomei AA, Siegert S, Britschgi MR, Luther SA, Swartz MA. Fluid flow regulates stromal cell organization and CCL21 expression in a tissue-engineered lymph node microenvironment. Journal of immunology. 2009;183(7):4273-83.
38. Valignat MP, Theodoly O, Gucciardi A, Hogg N, Lellouch AC. T lymphocytes orient against the direction of fluid flow during LFA-1-mediated migration. Biophysical journal. 2013;104(2):322-31.
39. Wucherpfennig KW, Gagnon E, Call MJ, Huseby ES, Call ME. Structural Biology of the T-cell Receptor: Insights into Receptor Assembly, Ligand Recognition, and Initiation of Signaling. Csh Perspect Biol. 2010;2(4).
40. Fuertes Marraco SA, Grosjean F, Duval A, Rosa M, Lavanchy C, Ashok D, et al. Novel murine dendritic cell lines: a powerful auxiliary tool for dendritic cell research. Frontiers in immunology. 2012;3:331.
41. Gopalakrishnan N, Hannam R, Casoni GP, Barriet D, Ribe JM, Haug M, et al. Infection and immunity on a chip: a compartmentalised microfluidic platform to monitor immune cell behaviour in real time. Lab on a chip. 2015;15(6):1481-7.
42. McDonald JC, Duffy DC, Anderson JR, Chiu DT, Wu H, Schueller OJ, et al. Fabrication of microfluidic systems in poly(dimethylsiloxane). Electrophoresis. 2000;21(1):27-40.
43. Rosa P, Tenreiro S, Chu V, Outeiro TF, Conde JP. High-throughput study of alpha-synuclein expression in yeast using microfluidics for control of local cellular microenvironment. Biomicrofluidics. 2012;6(1):14109-141099.
44. Mempel TR, Henrickson SE, Von Andrian UH. T-cell priming by dendritic cells in lymph nodes occurs in three distinct phases. Nature. 2004;427(6970):154-9.
45. Wang JH, Reinherz EL. A new angle on TCR activation. Immunity. 2011;35(5):658-60.
46. Wang JH, Reinherz EL. The structural basis of a ss T-lineage immune recognition: TCR docking topologies, mechanotransduction, and co-receptor function. Immunol Rev. 2012;250:102-19.
47. van der Merwe PA, Dushek O. Mechanisms for T cell receptor triggering. Nature reviews Immunology. 2011;11(1):47-55.
48. Staquet MJ, Jacquet C, Dezutter-Dambuyant C, Schmitt D. Fibronectin upregulates in vitro generation of dendritic Langerhans cells from human cord blood CD34+ progenitors. The Journal of investigative dermatology. 1997;109(6):738-43.
49. Lammermann T, Sixt M. The microanatomy of T-cell responses. Immunol Rev. 2008;221:26-43.
50. Celli S, Garcia Z, Bousso P. CD4 T cells integrate signals delivered during successive DC encounters in vivo. The Journal of experimental medicine. 2005;202(9):1271-8.
51. Alvarez D, Vollmann EH, von Andrian UH. Mechanisms and consequences of dendritic cell migration. Immunity. 2008;29(3):325-42.
52. Celli S, Garcia Z, Beuneu H, Bousso P. Decoding the dynamics of T cell-dendritic cell interactions in vivo. Immunol Rev. 2008;221:182-7.
53. Husson J, Chemin K, Bohineust A, Hivroz C, Henry N. Force Generation upon T Cell Receptor Engagement. PloS one. 2011;6(5).
54. Kim ST, Takeuchi K, Sun ZY, Touma M, Castro CE, Fahmy A, et al. The alphabeta T cell receptor is an anisotropic mechanosensor. The Journal of biological chemistry. 2009;284(45):31028-37.
55. Puech PH, Nevoltris D, Robert P, Limozin L, Boyer C, Bongrand P. Force Measurements of TCR/pMHC Recognition at T Cell Surface. PloS one. 2011;6(7).
56. Bird RB, Stewart WE, Lightfoot EN. Transport phenomena. 2nd, Wiley international ed. New York: J. Wiley; 2002. xii, 895 p. p.
57. Eich C, de Vries IJ, Linssen PC, de Boer A, Boezeman JB, Figdor CG, et al. The lymphoid chemokine CCL21 triggers LFA-1 adhesive properties on human dendritic cells. Immunology and cell biology. 2011;89(3):458-65.
58. Hoffmann S, Hosseini BH, Hecker M, Louban I, Bulbuc N, Garbi N, et al. Single cell force spectroscopy of T cells recognizing a myelin-derived peptide on antigen presenting cells. Immunology letters. 2011;136(1):13-20.
59. Mempel TR, Henrickson SE, von Andrian UH. T-cell priming by dendritic cells in lymph nodes occurs in three distinct phases. Nature. 2004;427(6970):154-9.